THERMODYNAMIC PERFORMANCE MAPS OF RECIPROCATING-PISTON EXPANDERS FOR OPERATION AT OFF-DESIGN AND PART-LOAD CONDITIONS

Simpson M., Rotolo G., Sapin P., De Palma P., White A.J. and Markides C.N.*
*Author for correspondence
Clean Energy Processes (CEP) Laboratory,
Department of Chemical Engineering,
Imperial College London,
London, United Kingdom.
E-mail: c.markides@imperial.ac.uk

ABSTRACT

Renewable energy sources, such as solar-thermal or geothermal heat, and low-/medium-grade industrial waste-heat can be converted into useful power and/or heating with a variety of technologies, including organic Rankine cycle (ORC) and vapour-compression heat-pump systems. The thermodynamic performance and cost of these technologies depends crucially on the efficiency of key components, including the compressor or expander used. Reciprocating-piston machines can be advantageous over turbomachines and other positive-displacement machines at intermediate scales (~10s-100s of kW) thanks to their ability to operate with relatively high isentropic efficiencies at large expansion ratios. However, modelling the thermodynamic losses in reciprocating-piston expanders, with a view towards designing high-performance machines, is a complex undertaking. The aim of this paper is to develop a spatially-lumped, yet dynamic model of a piston expander suitable for early-stage engineering design, that can provide simplification without sacrificing accuracy. The unsteady heat transfer between the gas and the cylinder walls, and the mass leakage are predicted independently with correlations available in the literature and simplified one-dimensional models, respectively. However, the turbulence induced by the mass intake through the piston rings can affect the gas-to-wall heat transfer. In order to address this dependency two complementary approaches are used. Compression and expansion processes are simulated in a gas spring configuration (i.e. without valve systems) using a computational fluid dynamics (CFD) model developed using the open-source code OpenFOAM, where the loss mechanisms are solved directly. The results are then compared with predictions from the heuristic lumped model based on heat transfer correlations. Finally, the lumped model is used to derive performance maps for a reciprocating-piston expander over a range of pressure ratios and mass flow rates.

NOMENCLATURE

A	[m^2], [Pa.s/K]	Area, Sutherland coefficient
$Co_{\max}$	[-]	Maximum Courant number
c_v	[J/(kg.K)]	Isochoric specific heat capacity
D_h	[m]	Hydraulic diameter
F	[Hz]	Piston oscillation frequency
H	[J/kg]	Specific enthalpy
$\dot{m}$	[kg/s]	Mass flow rate
Nu	[-]	Nusselt number
P	[Pa]	Pressure
Pe_ω	[-]	Peclet number
$\dot{Q}$	[W]	Heat flux
$\dot{q}$	[W/m^2]	Heat flux per unit area
R	[J/(kg.K)]	Specific gas constant
r_P	[-]	Pressure ratio
T	[K]	Temperature
t	[s]	Time
V	[m^3]	Volume
VR	[-]	Volume ratio
$\dot{W}$	[W]	Expander power output
x	[m]	Distance
y^+	[-]	Dimensionless wall distance

Greek characters

α	[m^2/s]	Thermal diffusivity
η	[-]	Expander efficiency
κ	[W/(m.K)]	Thermal conductivity
μ	[Pa.s]	Dynamic viscosity
ψ	[-]	Cyclic thermal loss coefficient
ω	[rad/s]	Rotational speed

Subscripts / Superscripts

$\mathcal{C}$	Complex	out	Exhaust
cr	Crankcase	$\mathcal{R}$	Real
cyl	Cylinder	s	Sutherland
dn	Downstream	up	Upstream
$\mathcal{I}$	Imaginary	w	Wall
in	Intake	vr	Valve restriction
is	Isentropic		

INTRODUCTION

The efficient and affordable use of renewable heat, such as solar-thermal or geothermal heat, and waste-heat from industrial processes via conversion to electricity or upgrading is an enabling element of a transition towards a decarbonised energy future. Organic Rankine cycle (ORC) and vapour-compression heat-pump systems have a role to play in this context, but the efficiency of such systems depends crucially on the performance of key components, including that of the compressor or expander. Other technologies which rely on imparting or extracting work to/from gases across temperature and pressure levels include compressed-air energy storage (CAES) and pumped-thermal energy storage (PTES) , which can help integrate intermittent sources of renewable energy into the grid.

At intermediate scales (~10s-100s of kW), reciprocating-piston machines have advantages over turbomachines and other positive-displacement machines that arise from their relatively high efficiencies, high pressure-ratio capabilities and robust part-load performance. However, pressure losses through the valves, gas-to-wall heat transfer, mass leakage and friction all act to limit expander efficiency. Careful valve design and timing strategies can be used to minimise pressure losses, while lubrication can be used to limit friction losses. On the other hand, the unsteady heat-

transfer between the gas and the cylinder walls, and the mass leakage of gas past the piston rings remain relatively challenging to predict and address. Therefore, these are at the focus of current efforts to enable the design of high-efficiency machines.

Heat transfer in piston machines has been the subject of many studies since the early work of Pfriem in 1940 . From this early work, it was understood that the unsteady component of the gas-to-wall heat transfer and, specifically, the effect of the compression/expansion work on the thermal boundary layer, leads to a phase shift between the bulk gas temperature and the heat flux during the cyclic operation of the machine, such that Newton's law of cooling ($\dot{Q} \propto \Delta T$) cannot adequately describe the heat transfer process in these systems. Therefore, Pfriem introduced a complex heat transfer coefficient in order to capture analytically both the magnitude of the heat transfer, and the phase difference between bulk gas temperature and the heat flux; the latter is a dominant factor in determining the exergy (or, useful work) losses associated with the heat exchange process within the compression or expansion space.

Lee considered a gas layer between oscillating parallel plates and developed an analytical model of a gas spring accounting for the aforementioned phase shift in heat transfer, and Kornhauser and Smith made a substantial contribution towards the understanding and description of this heat transfer process through a comprehensive experimental programme following the complex Nusselt number formulation pioneered by Lee [4]. Their semi-empirical correlation of Nusselt number against Peclet number, a non-dimensional frequency, showed good predictive ability for cycle-resolved heat flux in gas springs with low volume ratios. Lekic and Kok continued the work of Kornhauser, investigating in-cylinder conditions using direct numerical simulations (DNSs), which was compared with Kornhauser's experimental data and data from their own gas spring apparatus. The authors proposed a modification to earlier Nusselt number correlations based on their numerical results. Kornhauser's and Lekic's correlations are used in this work to select a suitable correlation for further modelling.

It is noted that both above correlations were developed for low volume-ratio machines, without significant mass leakage. Heat-flux measurements beyond these conditions were found to differ from predictions using these correlations and this aspect remains poorly understood, despite its clear and direct relevance in high volume-ratio practical applications. Furthermore, a coupling between heat transfer and mass leakage processes is anticipated, but the magnitude of this interaction is yet to be determined. It is expected that gas flow past the piston rings will influence the thermal boundary layer close to the piston head, potentially enhancing heat transfer, which will directly influence the exergy (work) losses in these machines.

NUMERICAL METHODS

The present paper reports on a numerical effort that employs on the open-source code OpenFOAM, following on from previous experimental studies by Sapin *et al*. in gas-spring systems. The numerical code used to perform the CFD investigations enables heat transfer and mass leakage to be simulated in detail. A zero-dimensional (spatially-lumped), dynamic model is also run in parallel to the CFD simulations, which employs the heat flux correlations from either Kornhauser and Smith or Lekic and Kok. The rapid running time of this model makes it well suited for design purposes, but the fidelity is reduced and the accuracy of its predictions not yet confirmed. The present study seeks to address these questions.

The modelled gas-spring geometry was taken from the earlier experimental work of Sapin *et al*. [8], who used a piston-cylinder arrangement with a cylinder bore of 105.0 mm, a connecting rod length of 148.5 mm and a piston stroke length of 77.8 mm. The clearance height was varied so as to achieve a desired volume ratio, between 77.8 mm (corresponding to a volume ratio of 2.0) and 14.05 mm (volume ratio of 6.5). The decision to vary the clearance height rather than the stroke length was made with future experimental campaigns in mind.

Dry air was used as the working fluid in a set of initial simulations, with properties derived from the NIST JANAF coefficients. The assumption is therefore that of semi-perfect gas, with specific heat capacities c_p and c_v that depend only on the temperature. The ideal gas equation was employed throughout this initial modelling effort.

Further, the Sutherland model was used for the evaluation of the dynamic viscosity μ, which calculates the temperature-dependent dynamic viscosity μ using two fluid parameters, the Sutherland coefficient A_s and the Sutherland temperature T_s:

$$\mu = \frac{A_s\sqrt{T}}{1 + T_s/T} \tag{1}$$

and the modified Eucken model was used for thermal conductivity:

$$\kappa = \mu c_v(1.32 - 1.77\frac{R}{c_v}) \tag{2}$$

The working fluid assumptions were applied identically in both the CFD and the lumped dynamic model.

CFD simulations

The open-source code OpenFOAM (v. 2.4.0) was used in this present study, employing a modified ColdEngineFoam solver. This solver provides inbuilt dynamic mesh controls to adjust for the changing volume in the cylinder. For full details of the CFD domain refer to Ref. . Briefly, the domain was a wedge subtending an angle of 0.02 rad (1.14°), one cell wide in the circumferential direction. Axisymmetric boundary conditions were applied to mimic full cylinder behaviour. This was checked in terms of global quantities of interest and found to be satisfactory. The number of cells required in the axial and radial directions is a function of the rotational speed being modelled: higher RPM simulations call for a larger number of cells. For a speed of 100 RPM, a mesh resolution of 150 × 150 was selected.

The simulation time-step was limited by a user-defined maximum Courant number Co_{max} value of 0.25:

$$Co_{\max} = \frac{|u|\Delta t}{\Delta x} \leq 0.25 \tag{3}$$

where u is the flow velocity, Δt is the timestep and Δx is the length of a given cell in the velocity direction. (N.B.: As the size of the mesh changes, Δx varies as well as the velocity.)

Several authors [7,9,10] have noted that the critical Reynolds number for transition from laminar to turbulent flow within oscillating cylinder flows has not been well defined. The DNSs performed by Lekic and Kok identified that laminar flows

dominated for $Re < 2500$. However, in order to capture the gas-spring's performance in both laminar and possible transition conditions, the $k-\omega$ SST turbulence model was selected, also since it was found that results from this model showed excellent agreement with data from laminar, low-speed experimental runs.

The boundary layer was resolved directly, i.e. without the use of wall functions, and the dimensionless wall distance y^+ was adjusted for each mesh, such that the value remained below unity. Comparisons between laminar and turbulent simulations showed minor differences at 1000 RPM, and larger variations beyond this.

Lumped model

By considering the gas in the cylinder as a single lumped mass, a simple model of an expander can be developed. Setting the inlet and exhaust valve flows to zero then allows a gas spring to be simulated, for comparison with the CFD simulations.

This model was implemented in MATLAB, and considers pressure P, temperature T and density ρ to be uniform throughout the cylinder. The model is dynamic, and computes a number of cycles until periodicity is achieved. The governing equations of mass and energy conservation are solved in a moving control volume $V(t)$, defined by the bore and the piston motion, as fixed by the stroke and connecting rod length.

Mass leakage sub-model

In both the CFD and the lumped model analyses, mass leakage to/from the cylinder past the piston rings was computed using a sub-model, operating in parallel with the main simulation. The sub-model calculates the mass flow between the cylinder and the crankcase, via a set of three crevices, as shown in Figure 1. This approach avoids the very fine mesh required to resolve the flows directly using OpenFOAM.

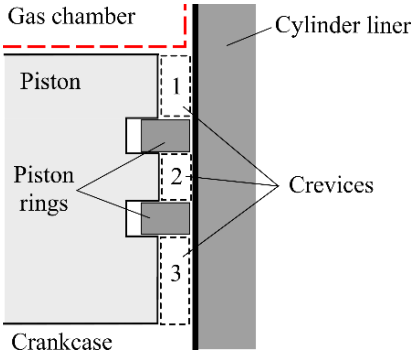

Figure 1 Piston detail showing crevices numbered 1-3

The large surface to volume ratio present in the crevices allows us to assume isothermal flow in these regions , as heat is exchanged rapidly between the cylinder walls, gas and piston. A pressure-driven model was defined in order to describe the mass exchange (flow) between the crevices:

$$P_1 = P_{\mathrm{cyl}} \tag{4}$$

$$\frac{\mathrm{d}P_2}{\mathrm{d}t} = \frac{T_2 R}{V_2}(\dot{m}_{21} + \dot{m}_{23}) \tag{5}$$

$$P_3 = P_{\mathrm{cr}} \tag{6}$$

where P_i is the pressure in crevice 'i', and 'cyl' and 'cr' refer to the cylinder and crankcase respectively. Mass transfer from Crevice 1 to 2, and from Crevice 3 to 2 are denoted $\dot{m}_{21}$ and $\dot{m}_{23}$ in turn. Each mass flow was treated as compressible and adiabatic (isentropic) flow through an orifice.

Equation (5) was solved using the 4th order Runge-Kutta method. Once the pressure in the second crevice was determined, the mass flow out of the cylinder $\dot{m}_{\mathrm{cyl}}$ was calculated:

$$\dot{m}_{\mathrm{cyl}} = \frac{V_1}{RT_1}\left(\frac{p_1^{n+1} - p_1^n}{\Delta t^{n+1}}\right) - \dot{m}_{12} \tag{7}$$

For the spatially-resolved CFD modelling, this was converted to a velocity boundary condition based on the conditions in either the cell closest to the wall or the crevice, depending on the direction of flow. The lumped model simply receives the change in mass and energy (enthalpy) directly.

Instantaneous heat transfer

Unsteady heat transfer between the gas and the cylinder walls continues to be challenging to both measure and predict. It is commonly assumed for modelling purposes that the cylinder wall temperature T_{w} is constant and uniform. For all simulations presented herein, T_{w} was fixed at 300 K.

The gas-to-wall heat transfer was handled differently in the CFD and lumped model approaches. Knowledge of spatially-resolved conditions from the CFD means that Fourier's Law can be applied locally at the wall:

$$\dot{q} = -\kappa \nabla T \tag{8}$$

The lumped model does not calculate the spatially-resolved temperature field, and hence relies on correlations developed for unsteady heat transfer under similar conditions.

The two correlations considered in this study were developed by Kornhauser and Smith (K&S) and Lekic and Kok (L&K). Both draw on a complex Nusselt approach, with geometry and operating speed characterised using the Peclet number Pe_ω:

$$Pe_\omega = \frac{\omega \overline{D_{\mathrm{h}}}^2}{4\alpha} \tag{9}$$

where ω is the crankshaft speed, $\overline{D_{\mathrm{h}}}$ is the cycle-averaged hydraulic diameter and α is the cycle-varying thermal diffusivity.

The complex Nusselt number Nu_c is a function only of Pe_ω. K&S defined the real and imaginary parts of Nu_c as:

$$Nu_{\Re} = Nu_{\Im} = 0.56 Pe_\omega^{0.69} \tag{10}$$

whereas L&K presented a modified version, where Nu_c is obtained using different real and imaginary parts:

$$Nu_{\Re} = 1.33 Pe_\omega^{0.56} + 5.36 \tag{11}$$

$$Nu_{\Im} = 2.04 Pe_\omega^{0.46} - 1.46 \tag{12}$$

The surface heat flux can then be defined using:

$$\dot{q}_w = -\frac{\kappa}{D_{\mathrm{h}}}\left[Nu_{\Re}(T - T_{\mathrm{w}}) + \frac{Nu_{\Im}}{\omega}\frac{\mathrm{d}(T - T_{\mathrm{w}})}{\mathrm{d}t}\right] \tag{13}$$

where κ is the instantaneous mass-averaged thermal conductivity of the fluid and D_{h} is the instantaneous hydraulic diameter in the

machine. The approach is concerned with the average heat flux across the cylinder area, notwithstanding that the cylinder head and piston will experience different heating profiles to the liner.

The correlations were developed for low volume ratios $VR = V_{BDC}/V_{TDC}$ of between 1.0 and 2.0. Simulations were also run at higher volume ratios to explore the breakdown of the correlations outside their region of validity.

CFD AND LUMPED MODEL COMPARISON

Results for the mass-averaged temperature and pressure inside the gas spring were compared, with excellent agreement in the peak pressure and temperature predictions from the CFD and the lumped model, which were found to be within 1% or better for a volume ratio of 2.0. Increasing the volume ratio to 6.5 led to discrepancies in peak pressure and temperature of up to 10% at higher RPM.

Predictions of heat transfer

The heat flux predicted by the CFD and the lumped model using each heat transfer correlation can be seen in Figure 2, for a volume ratio of 2.0 and a speed of 100 RPM. No mass leakage was simulated in this instance. This case was chosen to be broadly representative of the match between the approaches, though the magnitude of the discrepancy varies with speed.

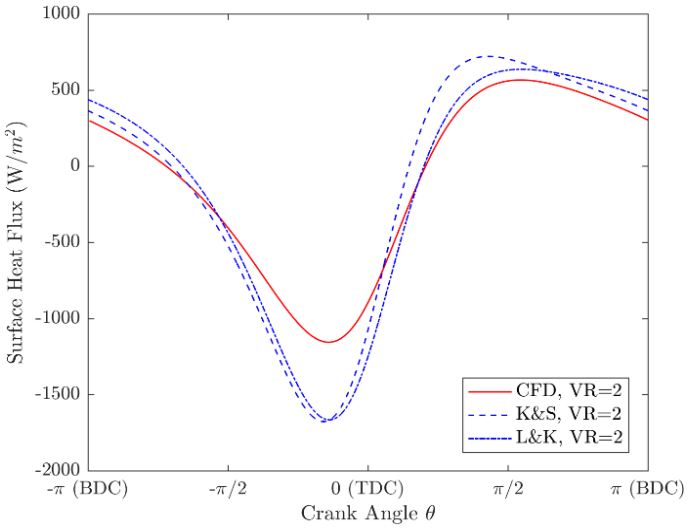

Figure 2 Surface heat-flux profile at 100 RPM for a volume ratio of 2.0, from CFD and lumped model with correlations

Both lumped model runs are found to overpredict the peak heat transfer from the gas to the walls by around 45%. The phase of this peak, however, shows good agreement across the three predictions, with each in the interval 25-29° before TDC.

Cyclic thermal loss

The non-dimensional loss due to heat transfer over a cycle can be described by the following thermal-loss expression:

$$\psi = \frac{\int \dot{Q}_w \, dt}{\frac{1}{2} \oint |P \, dV|} \qquad (14)$$

This thermal loss parameter ψ provides a useful indicator of how losses vary with Pe_ω, as shown in Figure 3 for volume ratios of 2.0 and 6.5. For $Pe_\omega > 10$, experimental work by Kornhauser identified that losses reduced in proportion to $Pe_\omega^{-0.5}$.

Referring to Figure 3 for the case of a volume ratio of 2.0, the trend in the cyclic loss from the CFD is best replicated by the lumped model with the L&K correlation. Both correlations show a gradient close to (–ve) 0.5, in agreement with Ref. . However, an offset exists, indicating a consistent overprediction of the loss by the lumped model. The slope of the loss predicted by the K&S correlation model is seen to deviate from the CFD.

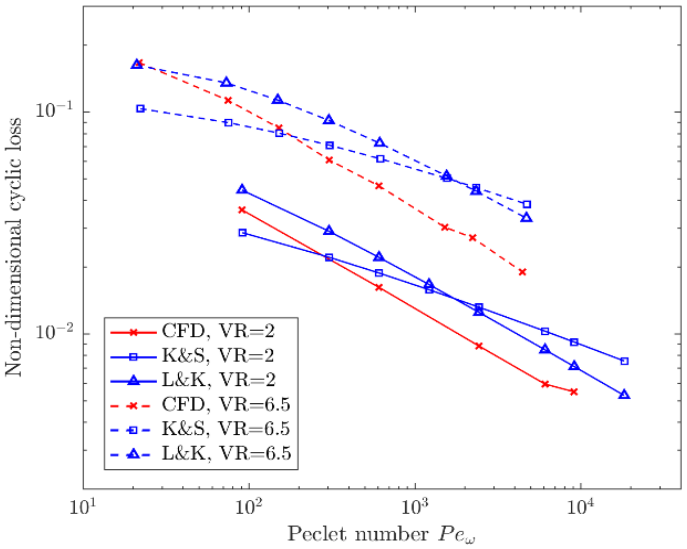

Figure 3 Variation of thermal cyclic loss with Pe_ω for volume ratios of 2.0 and 6.5, with no mass leakage

At a higher volume-ratio of 6.5, the agreement is less satisfactory, with neither correlation matching the slope obtained from the CFD, although the lumped model with the L&K correlation provides a closer approximation. This highlights the need for better understanding of high volume-ratios, particularly since this is of direct practical relevance for piston machines.

Effect of mass leakage

CFD simulations with and without mass leakage at 15 RPM and a volume ratio of 2.0 were compared. Both cases had the same average mass over a cycle. The comparison showed that including mass leakage resulted in a 24% higher total loss than the case without mass leakage. The increased loss was found to arise from the larger mass being compressed and the smaller mass being expanded, resulting in a greater net heat loss to the cylinder walls. The net effect of the enthalpy carried out of the cylinder by mass leakage was minor, representing just 0.2% of the total loss.

EXPANDER PERFORMANCE MAPS

In a final step, the lumped model presented above was used as a design tool to generate thermodynamic performance maps of a reciprocating-piston expander using R245fa (pentafluoropropane) as a working fluid. Unlike dry air, whose behaviour can be accurately described by the ideal gas law, R245fa exhibits significant compressibility effects. The thermophysical properties of this fluid depend both on pressure and temperature and were interpolated from the NIST database using the software REFPROP.

The piston-cylinder geometry is different from that used above, with a bore diameter of 60 mm, a stroke length of 57 mm, a connecting-rod length of 148.5 mm, and a clearance height of 10 mm. Intake and exhaust valves are also considered and the mass flow rates during the intake and exhaust strokes were calculated by solving the isentropic steady-flow energy equation across the valve restriction area A_{vr}:

$$\dot{m}_{in/out} = C_d \, \rho_{vr} \, A_{vr} \sqrt{2 \, (h_{up} - h_{vr})} \qquad (15)$$

$$h_{vr} = h \left(P_{dn}, S_{up} \right) \qquad (16)$$

where P_{dn} is the pressure downstream of the restriction, h_{up} and S_{up} are the specific enthalpy and entropy upstream of the valve. Irrecoverable losses due to real gas flow effects are included with the discharge coefficient C_d . In the system considered here, the intake valve opening spanned a range of 63°, starting from TDC, while the exhaust started at BDC for 126°.

The gas-to-wall heat transfer was calculated using the L&K correlation and the mass leakage through the piston rings was estimated with the sub-model presented in the previous section.

Two key parameters were varied in order to draw performance maps of the considered expander design, namely the crankshaft speed and the pressure ratio. Several pressure ratios r_P were imposed by varying the upstream pressure (with a constant 30 K superheat) while the downstream pressure was kept constant at 1.5 bar. The suction and discharge pressures were assumed to be constant during the cycle.

Several indicators can be defined to assess the performance of the expander design. The first indicator is the internal power output $\dot{W}$, i.e. the ratio of the net work done on the piston during one cycle multiplied by the frequency:

$$\dot{W} = f \cdot \oint P \, dV \qquad (17)$$

The expander isentropic efficiency η_{is} is the second performance indicator used in this study, defined as a comparison of the actual power with the isentropic case:

$$\eta_{is} = \frac{\dot{W}}{\dot{m}(h_{in} - h_{out,is})} \qquad (18)$$

where h_{in} is the gas enthalpy upstream of the expander and $h_{out,is}$ is the isentropic exhaust enthalpy, i.e. the gas enthalpy at the exhaust pressure P_{out} and at the intake specific entropy.

Figures 4 and 5 are the performance maps for the considered reciprocating-piston expander design, where the power output $\dot{W}$ and the isentropic efficiency η_{is} are plotted against the crankshaft rotational frequency ω and the imposed pressure ratio r_P. It is observed that $\dot{W}$ increases continuously with r_P, while η_{is} decreases with increasing r_P leading to an inevitable and important design trade-off. Increasing the pressure ratio, and hence the intake pressure, enhances the power production as more pressure is applied to the piston. Yet, it also gives rise to more thermodynamic losses as the mass leakage through the piston rings and the gas-to-wall heat transfer are enhanced due to higher pressure and temperature during the suction expansion stroke. These loss mechanisms reduce the thermodynamic efficiency of the engine due to exergy destruction and reduction in the work recovered by the piston at larger pressure ratios.

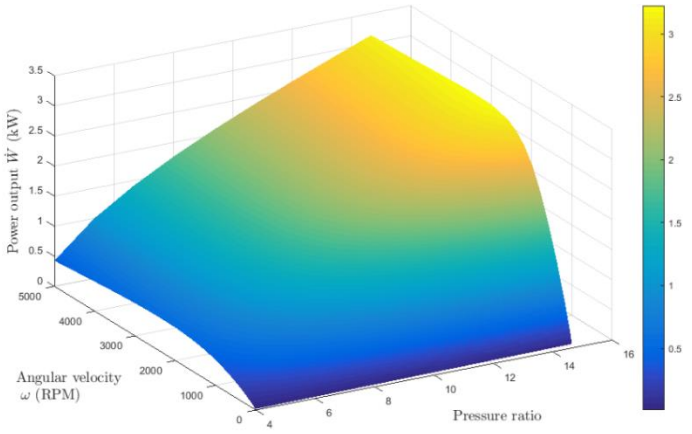

Figure 4 Expander power output as a function of frequency and pressure ratio; discharge pressure = 1.5 bar.

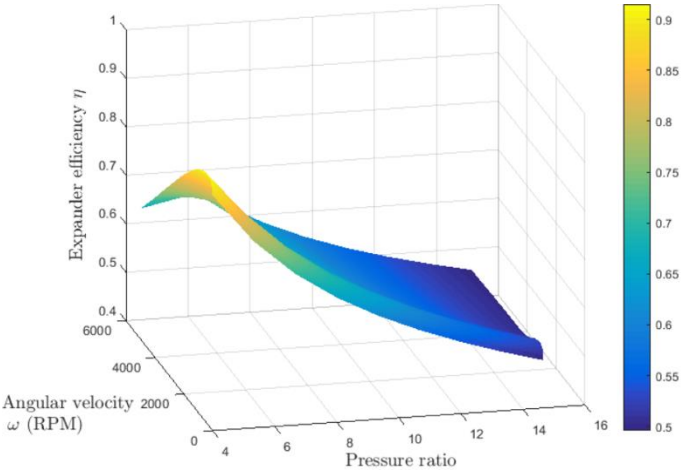

Figure 5 Expander isentropic efficiency as a function of frequency and pressure ratio; discharge pressure = 1.5 bar.

At a given pressure ratio, increasing the RPM has similar effects on the output work and the efficiency: both increase with the angular velocity up to a certain point (in the range 1000-1500 RPM in the present case, depending on r_P), then decrease at higher velocities. Throttling losses through the intake and exhaust valves are the reason for this limitation. The higher the RPM, the less time is available for the high-pressure vapour to fill in the chamber since the valve opening range is fixed. At high RPM, the pressure at the end of the intake stroke, i.e. before expansion, is less important than for lower RPM.

This can be clearly observed in Figure 6, where pressure-volume diagrams are plotted for a range of RPM, for a constant imposed pressure ratio of 8.0. It can be observed that the maximum pressure reached at 1400 RPM is significantly lower than the pressure reached at 15 RPM and 100 RPM, which almost equals the suction pressure of 12 bar.

The decrease in the work output with increasing RPM above a certain limit is associated with a decrease in the mass flow rate through the machine. In an ideal case (such as the dashed line in Figure 6), the total piston displacement is filled with gas at the intake condition and contains the maximum displacement mass, while the actual mass sucked into the piston in realistic cases is

lower. Hence, operation at higher RPM leads to lower volumetric efficiencies - defined as the ratio of the actual mass flow rate through the machine to the maximum possible flow rate.

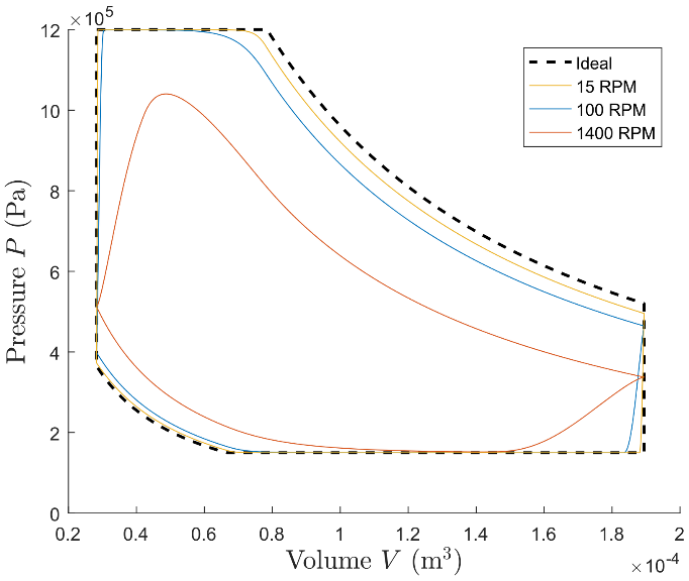

Figure 6 In-cylinder pressure-volume diagrams at 15, 100 and 1400 RPM; suction pressure = 12 bar, discharge pressure = 1.5 bar.

CONCLUSIONS

This paper presented a dynamic lumped model analysis of reciprocating-piston expander devices. In the first part, the predictions of the model in a gas-spring configuration were compared to fully-resolved CFD results. The comparison between the two models showed reasonable agreement and allowed us to select the Lekic and Kok correlation to estimate the gas-to-wall instantaneous heat transfer, on the understanding that losses were likely to be conservative. In the second part, performance maps of a reciprocating-piston expander were generated using the lumped model. As expected, the power output increases continuously with the pressure ratio. It is optimal for a specific RPM, as is the case for the isentropic efficiency. The latter, however, decreases continuously with pressure ratio, due to declining volumetric efficiency. This numerical model can be used as a design tool and allows prediction of the thermodynamic performance of piston expanders at off-design and part-load conditions.

ACKNOWLEDGEMENTS

This work was supported by the UK Engineering and Physical Sciences Research Council (EPSRC) [grant numbers EP/P004709/1 and EP/J006041/1]. Data supporting this publication can be obtained on request from cep-lab@imperial.ac.uk.

REFERENCES

[1] J. Freeman, K. Hellgardt and C. N. Markides, "An assessment of solar-powered organic Rankine cycle systems for combined heating and power in UK domestic applications," *Applied Energy*, vol. 138, pp. 605-620, 2015.

[2] A. J. White, G. Parks and C. N. Markides, "Thermodynamic analysis of pumped thermal electricity storage," *Applied Thermal Engineering*, vol. 53, no. 2, pp. 291-298, 2013.

[3] H. Pfriem, "Periodic heat transfer at small pressure fluctuations," 1943.

[4] K. P. Lee, "A simplistic model of cyclic heat transfer phenomena in closed spaces," in *Proceedings of the Eighteenth Intersociety Energy Conversion Engineering Conference*, Orlando, Florida, 1983.

[5] A. A. Kornhauser and J. L. Smith, "Application of a complex Nusselt number to heat transfer during compression and expansion," *Journal of heat transfer*, vol. 116, no. 3, pp. 536-542, 1994.

[6] U. Lekic and J. B. W. Kok, "Heat transfer and fluid flows in gas springs," *Open Thermodynamics Journal*, vol. 4, pp. 13-26, 2010.

[7] U. Lekic, "Fluid flow and heat transfer in a helium gas spring," 2011.

[8] P. Sapin, A. I. Taleb, C. Barfuss, A. J. White and C. N. Markides, "Thermodynamic Losses in a Gas Spring: Comparison of Experimental and Numerical Results," in *12th International Conference on Heat Transfer, Fluid Mechanics and Thermodynamics*, Malaga, Spain, 2016.

[9] A. I. Taleb, P. Sapin, C. Barfuss, A. J. White, D. Fabris and C. N. Markides, "Wall temperature and system mass effects in a reciprocating gas spring," in *Proceedings of ECOS 2016*, Portoroz, Slovenia, 2016.

[10] A. A. Kornhauser, "Gas-wall heat transfer during compression and expansion," 1989.

[11] M. Namazian and J. Heywood, "Flow in the Piston-Cylinder-Ring Crevices of a Spark-Ignition Engine: Effect on Hydrocarbon Emissions, Efficiency and Power," 1982.

[12] A. A. Kornhauser and J. Smith Jr., "The Effects of Heat Transfer on Gas Spring Performance," *ASME DC Journal of Energy Resources Technology*, vol. 115, pp. 70-75, 1993.

[13] J. Heywood, Internal Combustion Engine Fundamentals, McGraw-Hill Education, 1988.